IEEE Access
Multidisciplinary | Rapid Review | Open Access Journal

Received July 23, 2020, accepted August 2, 2020, date of publication August 5, 2020, date of current version August 17, 2020.

Digital Object Identifier 10.1109/ACCESS.2020.3014303

Envelope Level Crossing Rate and Average Fade Duration of a Generic 3D Non-Stationary UAV Channel Model

QIUMING ZHU[1], (Member, IEEE), NENG CHENG[1], XIAOMIN CHEN[1], (Member, IEEE), WEIZHI ZHONG[2], (Member, IEEE), BOYU HUA[1], AND YAWEN WANG[1]

[1]Key Laboratory of Dynamic Cognitive System of Electromagnetic Spectrum Space, College of Electronic and Information Engineering, Nanjing University of Aeronautics and Astronautics, Nanjing 211106, China
[2]Key Laboratory of Dynamic Cognitive System of Electromagnetic Spectrum Space, College of Astronautics, Nanjing University of Aeronautics and Astronautics, Nanjing 211106, China

Corresponding authors: Qiuming Zhu (zhuqiuming@nuaa.edu.cn) and Xiaomin Chen (chenxm402@nuaa.edu.cn)

This work was supported in part by the National Key Scientific Instrument and Equipment Development Project under Grant 61827801; in part by the Aeronautical Science Foundation of China under Grant 201901052001; in part by the Fundamental Research Funds for the Central Universities under Grant NS2020026 and Grant NS2020063; and in part by the Open Foundation for Graduate Innovation of the Nanjing University of Aeronautics and Astronautics under Grant KFJJ 20190418.

ABSTRACT For the unmanned aerial vehicle (UAV) communication scenarios, the time-varying fading characteristics cased by the three-dimensional(3D) scattering environment and 3D trajectory have an important impact on establishing the reliable communication link. In this paper, a generic 3D non-stationary geometry-based stochastic model (GBSM) for UAV channels is developed. Different from the traditional 3D GBSMs, the proposed model takes the 3D arbitrary trajectories of UAV into account. On this basis, two important second-order statistical properties of fading envelope, i.e., the level crossing rate (LCR) and average fading duration (AFD), are investigated and derived in details. The obtained closed-form expressions are explicit functions of flight parameters and compatible with the results in the previous works. Numerical simulations show that the simulated results are in accordance with the theoretical and measurement data under 3D flight scenarios. The proposed model and statistical properties can be applied to the optimal design of channel coding and block interleave schemes for UAV communication systems.

INDEX TERMS Unmanned aerial vehicle (UAV) channel, channel model, fading envelope, level crossing rate (LCR), average fading duration (AFD).

I. INTRODUCTION

Unmanned aerial vehicles (UAVs) have been attracting more and more attention in the military and civilian fields, such as weather monitoring, forest fire detection, filming, goods transport, and traffic control, for their affordable prices and high flexibility [1]. The UAV-assisted communications have been considered as an important option in the fifth generation (5G) communication systems [2], [3] and are also essential for extending wireless network coverage and relay communications [4], [5].

Due to the high-altitude and high-speed flight of UAV, the propagation environment of UAV communication is quite different from the conventional cellular and vehicular communications [6]. For example, the Doppler frequency changes rapidly due to the three-dimensional (3D) movement of UAV in the 3D space. This would lead to the severe fluctuation of received power and the deterioration of system performance [7], [8]. Therefore, a thorough understanding of UAV channel and its characteristics is vital to guarantee the high-speed transmission and reliability requirements of UAV communication systems. Particularly, it is a hot topic to investigate the statistical properties of UAV channels, such as probability distribution function (PDF), autocorrelation function (ACF), cross-correlation function (CCF), Doppler power spectral density (DPSD), level crossing rate (LCR), and average fade duration (AFD) [9]–[13]. Note that LCR and AFD are two important second-order statistical properties reflecting the fluctuation of fading envelope over time, and they have an important impact on the channel coding

The associate editor coordinating the review of this manuscript and approving it for publication was Jiayi Zhang.

and block interleave schemes. However, the investigations of LCR and AFD for UAV channels are very limited compared with other statistical properties.

The existing UAV channel models in the literatures can be classified into two categories, the deterministic model and the stochastic model. Several typical deterministic models, e.g., the Ray-tracing model and finite-difference time domain (FDTD) model can be addressed in [14]–[17]. Due to the advantages of generality and complexity, most of research work was focused on the stochastic models, which can be further categorized into the non-geometrical stochastic models (NGSMs) [18]–[22] and geometry-based stochastic models (GBSMs) [23]–[30], e.g., sphere model, cylinder model, two-cylinder model, and etc. In [23], the authors proposed a UAV channel model with cylindrical scatterers including the line of sight (LoS) and non-line-of-sight (NLoS) paths, and investigated the relevance between the position and flight direction of UAV with the channel space-time frequency correlation characteristics. In [24], [25], the authors analyzed the influence of azimuth angle of arrival (AAOA) and elevation angle of arrival (EAOA) on the space-time correlation characteristics of a cylinder GBSM UAV channel model, but the analysis of LCR and AFD was missing in these articles. Based on the sphere GBSM channel model, the authors in [26] derived the expressions of second-order statistical properties, which showed LCR was positively correlated with the carrier frequency. In [27], a 3D cylinder GBSM for UAV channels was proposed and the influence of the Rice factor, angle of arrival (AOA), and angle of departure (AOD) on the LCR and AFD was investigated. Furthermore, the authors in [28] derived the explicit expressions of LCR and AFD, but the UAV was assumed flying with a constant speed. In [29], the LCR and AFD were analyzed based on the hemispherical channel model, but no detailed derivation was given and the model was also lacked of generality. In [30], the cylinder channel model proposed by the authors researched the ACF, CCF, DPSD, but neglected the analysis of LCR and AFD only giving the final results. Overall, a thorough exploitation of LCR and AFD for generic 3D non-stationary channels is still challenging. This paper aims to fill this research gap and the primary contributions are summarized as follows:

1) A general 3D non-stationary UAV communication channel model in the 3D space is developed. The new channel model originates from the conventional GBSM but considers the effect of 3D scattering environment and 3D arbitrary trajectory of transceivers on the time-varying characteristics.

2) The expressions of joint fading PDF, Doppler frequency, and ACF of proposed channel model are derived. On this basis, the LCR and AFD of fading envelope are analyzed and the corresponding theoretical expressions including the effect of 3D flight parameters are given. The theoretical results are also compared with the simulated and measured ones to verify the correctness of proposed model and derivations.

The reminder of this paper is structured as follows. In Section II, a generic 3D non-stationary UAV channel model is proposed. The joint PDF of channel fading envelope, Doppler frequency, ACF, LCR, and AFD are derived in Section III. Simulations are performed and compared with the theoretical results in Section IV. Finally, conclusions are given in Section V.

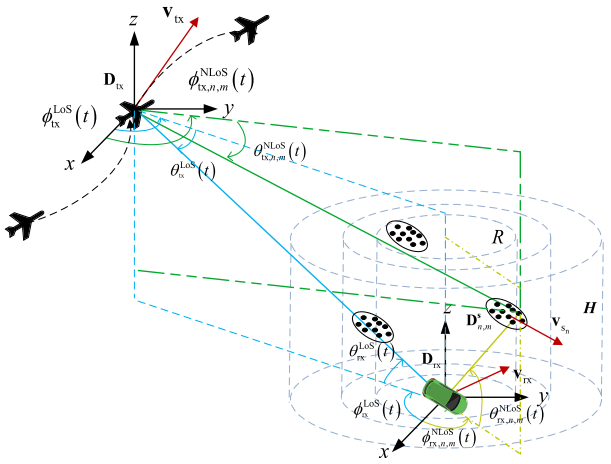

FIGURE 1. 3D non-stationary GBSM for UAV channels.

II. A GENERIC 3D NON-STATIONARY GBSM FOR UAV CHANNELS

A representative communication link between the UAV and vehicle is shown in Fig. 1. Both the UAV and vehicle are moving with 3D velocities, denoted as $\mathbf{v}_{tx}(t)$ and $\mathbf{v}_{rx}(t)$, respectively. Due to the high-altitude flight of UAV, the valid clusters are only existing around the vehicle. It's assumed that the nth cluster, denoted by S_n, consists of M randomly distributed scatterers and locates on the surface of one of several circular cylinders with radius R and height H as shown in Fig. 1. The detailed parameters are shown in Table 1. Note that the spherical unit vector in the 3D space is defined as

$$\mathbf{s}(v(t), u(t)) = \begin{bmatrix} \cos v(t) \cos u(t) \\ \cos v(t) \sin u(t) \\ \sin v(t) \end{bmatrix}, \tag{1}$$

where $v(t)$ and $u(t)$ denotes the azimuth and elevation angle, respectively. Thus, $\mathbf{s}_{tx/rx}^{v}(t)$, $\mathbf{s}_{tx/rx}^{LoS}(t)$, and $\mathbf{s}_{tx/rx,n,m}(t)$ can be respectively obtained by $\mathbf{s}(\beta_{tx/rx}(t), \alpha_{tx/rx}(t))$, $\mathbf{s}\left(\theta_{tx/rx}^{LoS}(t), \phi_{tx/rx}^{LoS}(t)\right)$, and $\mathbf{s}\left(\theta_{tx/rx,n,m}^{NLoS}(t), \phi_{tx/rx,n,m}^{NLoS}(t)\right)$, while $\mathbf{v}_{tx/rx}(t)$ can be written as $\|\mathbf{v}_{tx/rx}(t)\| \cdot \mathbf{s}(\beta_{tx/rx}(t), \alpha_{tx/rx}(t))^T$.

The small scale fading channel between the UAV and vehicle i.e., the channel impulse response (CIR) $\tilde{H}(\tau, t)$, can be represented by the combination of LoS component and several NLoS components as

$$\tilde{H}(\tau, t) = \sqrt{\frac{1}{K_R(t)+1}} \sum_{n=1}^{N} \tilde{H}_n^{NLoS}(t)\, \delta(\tau - \tau_n(t)) + \sqrt{\frac{K_R(t)}{K_R(t)+1}} \tilde{H}^{LoS}(t)\, \delta(\tau - \tau(t)), \tag{2}$$

TABLE 1. The channel parameters.

Parameter	Definition
$\mathbf{v}_{\mathrm{tx}}(t), \mathbf{v}_{\mathrm{rx}}(t)$	3D velocity vectors of the UAV and vehicle, respectively
$\alpha_{\mathrm{tx/rx}}(t), \beta_{\mathrm{tx/rx}}(t)$	Azimuth and elevation angles of the velocity vectors of the UAV and vehicle, respectively
$\phi^{\mathrm{LoS}}_{\mathrm{tx/rx}}(t), \theta^{\mathrm{LoS}}_{\mathrm{tx/rx}}(t)$	Azimuth and elevation angles of departure/arrival signal of the LoS path, respectively
$\phi^{\mathrm{NLoS}}_{\mathrm{tx/rx},n,m}(t), \theta^{\mathrm{NLoS}}_{\mathrm{tx/rx},n,m}(t)$	Azimuth and elevation angles of departure/arrival of the mth ray within the nth NLoS path, respectively
$\mathbf{s}^{v}_{\mathrm{tx}}(t), \mathbf{s}^{v}_{\mathrm{rx}}(t)$	Spherical unit vectors of the velocity of UAV and vehicle, respectively
$\mathbf{s}^{\mathrm{LoS}}_{\mathrm{tx}}(t), \mathbf{s}^{\mathrm{LoS}}_{\mathrm{rx}}(t)$	Spherical unit vectors of the LoS path of departure and arrival signals, respectively
$\mathbf{s}_{\mathrm{tx},n,m}(t), \mathbf{s}_{\mathrm{rx},n,m}(t)$	Spherical unit vectors of the mth ray within the nth NLoS path of departure and arrival signals, respectively

where N is the number of valid NLoS components, $K_R(t)$ represents the Ricean K-factor, $\tau(t)$ and $\tau_n(t)$ denote the delay of LoS component and the nth NLoS component respectively. The LoS and NLoS components of CIR can be further respectively expressed as

$$\tilde{H}^{\mathrm{LoS}}(t) = e^{j\left[\int_0^t k\left(\mathbf{v}_{\mathrm{tx}}(\tau)\cdot\mathbf{s}^{\mathrm{LoS}}_{\mathrm{tx}}(\tau)+\mathbf{v}_{\mathrm{rx}}(\tau)\cdot\mathbf{s}^{\mathrm{LoS}}_{\mathrm{rx}}(\tau)\right)d\tau+\varphi^{\mathrm{LoS}}\right]} \quad (3)$$

and (4), as shown at the bottom of the page, where $k = 2\pi f_0/\mathrm{c}_0$ denotes the wave number, f_0 and c_0 represent the carrier frequency and the speed of light, respectively, $\sqrt{P_n}$ means the power, $h_n^{\mathrm{NLoS}}(t)$ is the complex channel coefficient, M is the number of rays, φ^{LoS} and $\varphi_{n,m}$ are the random initial phases of LoS and NLoS components.

III. THEORETICAL DERIVATION OF LCR AND AFD

A. JOINT PDFs OF FADING ENVELOPE

Since the LoS component can be regarded as a special case of NLoS component containing one sub-path, hereafter we take the NLoS component as an example to derive the theoretical expressions of statistical properties. Firstly, the $h_n^{\mathrm{NLoS}}(t)$ can be rewritten as the inphase component and quadrature component as

$$h_n^{\mathrm{NLoS}}(t) = h_{1,n}^{\mathrm{NLoS}}(t) + jh_{2,n}^{\mathrm{NLoS}}(t), \quad (5)$$

and the envelope is denoted as $\varsigma = \left|h_n^{\mathrm{NLoS}}(t)\right|$. At the time instant of $t = t_0$, we have

$$\begin{aligned} h_{1,n}^{\mathrm{NLoS}}(t_0) &= \sqrt{\frac{1}{M}}\sum_{m=1}^{M}\cos\left(\Phi^{\mathrm{NLoS}}(t_0)+\varphi_{n,m}\right) \\ h_{2,n}^{\mathrm{NLoS}}(t_0) &= \sqrt{\frac{1}{M}}\sum_{m=1}^{M}\sin\left(\Phi^{\mathrm{NLoS}}(t_0)+\varphi_{n,m}\right), \end{aligned} \quad (6)$$

where

$$\Phi^{\mathrm{NLoS}}(t_0) = k\cdot\int_0^{t_0}\mathbf{v}_{\mathrm{tx}}(\tau)\cdot\mathbf{s}_{\mathrm{tx},n,m}(\tau)+\mathbf{v}_{\mathrm{rx}}(\tau)\cdot\mathbf{s}_{\mathrm{rx},n,m}(\tau)\,d\tau. \quad (7)$$

According to [31, Eq.(17)], the envelope distributions of $h_{1,n}^{\mathrm{NLoS}}$ and $h_{2,n}^{\mathrm{NLoS}}$ can be derived as

$$p_{h_{i,n}^{\mathrm{NLoS}}}(x_i) = \begin{cases} \dfrac{\sqrt{m}}{\pi\sqrt{1-mx_i^2}}, & |x_i| < \dfrac{1}{\sqrt{m}} \\ 0, & |x_i| \geq \dfrac{1}{\sqrt{m}}, \end{cases} \quad (8)$$

where $i = 1, 2$. It is noticed that $h_{1,n}^{\mathrm{NLoS}}(t_0)$ and $h_{2,n}^{\mathrm{NLoS}}(t_0)$ are statistically dependent, thus the joint PDF can be expressed as

$$p_{h_{1,n}^{\mathrm{NLoS}}h_{2,n}^{\mathrm{NLoS}}}(x_1, x_2) = p_{h_{1,n}^{\mathrm{NLoS}}}(x_1)\cdot\delta\left(x_2 - g(x_1)\right), \quad (9)$$

where

$$g(x_1) = \begin{cases} \sqrt{1/m - x_1^2}, & |x_1| \leq \sqrt{1/m} \\ 0, & |x_1| > \sqrt{1/m}. \end{cases} \quad (10)$$

Secondly, the joint characteristic function of $h_{1,n}^{\mathrm{NLoS}}(t_0)$ and $h_{2,n}^{\mathrm{NLoS}}(t_0)$ can be derived as

$$\Psi_{\hat{h}_{1,n}^{\mathrm{NLoS}}\hat{h}_{2,n}^{\mathrm{NLoS}}}(\nu_1, \nu_2) = \prod_{m=1}^{M} J_0\left(2\pi\frac{1}{\sqrt{m}}\sqrt{\nu_1^2+\nu_2^2}\right), \quad (11)$$

where $J_0(\cdot)$ denotes the first class of zero-order Bessel function. Making the Fourier transform on (11), we can obtain

$$\tilde{H}_n^{\mathrm{NLoS}}(t) = \sqrt{P_n}h_n^{\mathrm{NLoS}}(t) = \sqrt{\frac{P_n}{M}}\sum_{m=1}^{M} e^{j\left[\int_0^t k\left(\mathbf{v}_{\mathrm{tx}}(\tau)\cdot\mathbf{s}_{\mathrm{tx},n,m}(\tau)+\mathbf{v}_{\mathrm{rx}}(\tau)\cdot\mathbf{s}_{\mathrm{rx},n,m}(\tau)\right)d\tau+\varphi_{n,m}\right]} \quad (4)$$

the joint PDF of $h_{1,n}^{\mathrm{NLoS}}(t)$ and $h_{2,n}^{\mathrm{NLoS}}(t)$ as

$$p_{\hat{h}_{1,n}^{\mathrm{NLoS}}\hat{h}_{2,n}^{\mathrm{NLoS}}}(x_1,x_2) = 2\pi\int_0^{\infty}\left[J_0\left(2\pi\frac{1}{\sqrt{m}}r\right)\right]\cdot J_0\left(2\pi r\sqrt{x_1^2+x_1^2}\right)rdr. \tag{12}$$

By transforming the Cartesian coordinate (x_1, x_2) into the polar coordinate (z, θ) where $x_1 = z\cos\theta$ and $x_2 = z\sin\theta$, which yields the joint PDF of fading envelope and phase as

$$\begin{aligned} p_{\varsigma\vartheta}(z,\theta) &= z p_{\hat{h}_{1,n}^{NLoS}\hat{h}_{2,n}^{NLoS}}(z\sin\theta, z\cos\theta) \\ &= 2\pi z\int_0^{\infty}\left[J_0\left(2\pi\frac{1}{\sqrt{m}}x\right)\right]\cdot J_0(2\pi xz)\,xdx. \end{aligned} \tag{13}$$

On this basis, we can get the PDF of fading envelope by integrating (13) over $\theta \in (-\pi, \pi)$ as

$$p_{\varsigma}(r) = (2\pi)^2 r\int_0^{\infty}\left[\prod_{m=1}^{M}J_0\left(2\pi\frac{1}{\sqrt{m}}x\right)\right]J_0(2\pi rx)\,xdx. \tag{14}$$

Finally, the joint PDF of ς and its first derivative, which will be used in the following derivation, can be obtained as (15), as shown at the bottom of the page.

B. TIME-VARIANT DOPPLER FREQUENCY

The Doppler frequency shift (or Doppler frequency for brief) caused by the movements of terminals is closely related to the channel fading characteristic. Actually, the Doppler frequency is a function of velocities and spherical unit vectors of departure and arrival signals. In this section, we take the NLoS component as an example to analyze the Doppler frequency, which is theoretically defined as (16), as shown at the bottom of the page, where $\lambda = c_0/f_0$ means the wavelength. Due to the fast movement of UAV, the relative locations of UAV, vehicle and scatterers change over time, and this would lead to the obvious non-stationarity of the UAV channel. Note that some existing non-stationary channel models [32] directly used the following item to calculate the phase caused by the Doppler frequency under non-stationary scenarios

$$\Phi^{\mathrm{NLoS}'}(t) = k\cdot\left[\mathbf{v}_{\mathrm{tx}}(\tau)\cdot\mathbf{s}_{\mathrm{tx},n,m}(\tau)+\mathbf{v}_{\mathrm{rx}}(\tau)\cdot\mathbf{s}_{\mathrm{rx},n,m}(\tau)\right]t. \tag{17}$$

However, according to the relationship between frequency and phase, the output Doppler frequency can be calculated as

$$\begin{aligned} f_{n,m}^{\mathrm{NLoS}'}(t) &= \frac{1}{2\pi}\frac{d\Phi^{\mathrm{NLoS}'}(t)}{dt} \\ &= \frac{1}{\lambda}\left[\mathbf{v}_{\mathrm{tx}}(t)\cdot\mathbf{s}_{\mathrm{tx},n,m}(t)+\mathbf{v}_{\mathrm{rx}}(t)\cdot\mathbf{s}_{\mathrm{rx},n,m}(t)\right. \\ &\quad \left.+\frac{d\left(\mathbf{v}_{\mathrm{tx}}(t)\cdot\mathbf{s}_{\mathrm{tx},n,m}(t)+\mathbf{v}_{\mathrm{rx}}(t)\cdot\mathbf{s}_{\mathrm{rx},n,m}(t)\right)}{dt}t\right] \neq f_{n,m}^{\mathrm{NLoS}}(t). \end{aligned} \tag{18}$$

which is inconsistent with the theoretical one as (16). In contrast, for the proposed model in this paper, the output Doppler frequency exactly equals to the theoretical one as

$$\begin{aligned} f_{n,m}^{\mathrm{NLoS}}(t) &= \frac{1}{2\pi}\frac{d\Phi^{\mathrm{NLoS}}(t)}{dt} \\ &= \frac{1}{\lambda}\left[\mathbf{v}_{\mathrm{tx}}(t)\cdot\mathbf{s}_{\mathrm{tx},n,m}(t)+\mathbf{v}_{\mathrm{rx}}(t)\cdot\mathbf{s}_{\mathrm{rx},n,m}(t)\right]. \end{aligned} \tag{19}$$

Moreover, the new model also supports velocity variations as well as arbitrary trajectories of terminals.

During the short time period, both the UAV and vehicle can be viewed as moving on a horizontal plane. For this reason, the theoretical Doppler frequency can be simplified as (20), as shown at the bottom of the next page. Furthermore, if the movement of vehicle is ignored and the elevation angle of transmitting signal from the UAV is fixed in the 2D scenario,

$$\begin{aligned} p_{\varsigma\dot{\varsigma}}(t,r,\dot{r}) = 4\pi r\int_0^{\infty}\int_0^{\infty}\int_0^{2\pi}\left[\prod_{m=1}^{M}J_0\left(\frac{1}{\sqrt{m}}\left\{r_1{}^2+\left(2\pi\dot{\Phi}^{\mathrm{NLoS}}(t)\,r_2\right)^2\right.\right.\right. \\ \left.\left.\left.-4\pi\dot{\Phi}^{\mathrm{NLoS}}(t)\,r_1r_2\sin\theta\right\}^{1/2}\right)\right]\cdot\mathrm{e}^{-j2\pi[rr_1\cos\theta+\dot{r}r_2]}r_1d\theta dr_1dr_2 \end{aligned} \tag{15}$$

$$\begin{aligned} f_{n,m}^{\mathrm{NLoS}}(t) &= \frac{1}{\lambda}\left(\mathbf{v}_{\mathrm{tx}}(t)\cdot\mathbf{s}_{\mathrm{tx},n,m}(t)+\mathbf{v}_{\mathrm{rx}}(t)\cdot\mathbf{s}_{\mathrm{rx},n,m}(t)\right) \\ &= \frac{1}{\lambda}\left(\|\mathbf{v}_{\mathrm{tx}}(t)\|\begin{bmatrix}\cos\beta_{\mathrm{tx}}(t)\cos\alpha_{\mathrm{tx}}(t)\\ \cos\beta_{\mathrm{tx}}(t)\sin\alpha_{\mathrm{tx}}(t)\\ \sin\beta_{\mathrm{tx}}(t)\end{bmatrix}^T\cdot\begin{bmatrix}\cos\theta_{\mathrm{tx},n,m}^{\mathrm{NLoS}}(t)\cos\phi_{\mathrm{tx},n,m}^{\mathrm{NLoS}}(t)\\ \cos\theta_{\mathrm{tx},n,m}^{\mathrm{NLoS}}(t)\sin\phi_{\mathrm{tx},n,m}^{\mathrm{NLoS}}(t)\\ \sin\theta_{\mathrm{tx},n,m}^{\mathrm{NLoS}}(t)\end{bmatrix}\right. \\ &\quad \left.+\|\mathbf{v}_{\mathrm{rx}}(t)\|\begin{bmatrix}\cos\beta_{\mathrm{rx}}(t)\cos\alpha_{\mathrm{rx}}(t)\\ \cos\beta_{\mathrm{rx}}(t)\sin\alpha_{\mathrm{rx}}(t)\\ \sin\beta_{\mathrm{rx}}(t)\end{bmatrix}^T\cdot\begin{bmatrix}\cos\theta_{\mathrm{rx},n,m}^{\mathrm{NLoS}}(t)\cos\phi_{\mathrm{rx},n,m}^{\mathrm{NLoS}}(t)\\ \cos\theta_{\mathrm{rx},n,m}^{\mathrm{NLoS}}(t)\sin\phi_{\mathrm{rx},n,m}^{\mathrm{NLoS}}(t)\\ \sin\theta_{\mathrm{rx},n,m}^{\mathrm{NLoS}}(t)\end{bmatrix}\right) \end{aligned} \tag{16}$$

the Doppler frequency can be further simplified as

$$f_{n,m}^{\mathrm{NLoS}}(t)=\frac{1}{\lambda}\cdot\|\mathbf{v}_{\mathrm{tx}}(t)\|\cos\left[\alpha_{\mathrm{tx}}(t)-\phi_{\mathrm{tx},n,m}^{\mathrm{NLoS}}(t)\right], \quad (21)$$

and this special case can be addressed in [33].

C. CLOSED-FORM EXPRESSIONS OF ACF

The normalized spatial-temporal correlation function of proposed channel model can be defined as

$$\rho(\Delta f,\Delta t;t)=E\left\{\frac{H^{*}(t)H(\Delta f,t+\Delta t)}{|H^{*}(t)|\,|H(\Delta f,t+\Delta t)|}\right\}, \quad (22)$$

where $(\cdot)^{*}$ denotes the conjugate and $H(f,t)$ denotes the Fourier transform of CIR. Due to the non-stationarity of UAV channel, this paper divides the whole channel into several time intervals and assumes that the channel keeps stationary within each short time interval. By setting $\Delta f=0$ in (22), the ACF can be expressed as (23), as shown at the bottom of the page.

Referring to the measurements and recommendations of standardized channel models in [34], this paper describes the elevation and azimuth angles by the Laplacian distribution and VM distribution, respectively. Under non-stationary scenarios, the corresponding PDFs should be time-variant and expressed respectively as

$$f(\theta,t)=\frac{1}{2\sigma}\mathrm{e}^{-\frac{|\theta(t)-\bar{\theta}(t)|}{\sigma}} \quad (24)$$

and

$$f(\phi,t)=\frac{\mathrm{e}^{\kappa\cos(\phi(t)-\bar{\phi}(t))}}{2\pi I_0(\kappa)} \quad (25)$$

where $\bar{\theta}(t)$ and $\bar{\phi}(t)$ denotes the mean values of elevation and azimuth angles, respectively, and $I_0(\cdot)$ is the zeroth-order modified Bessel function of the first kind, and σ and κ control the angle spread on the elevation and azimuth planes, respectively. Then, the time-variant elevation and azimuth angles are modeled as

$$\theta_{\mathrm{tx/rx},n,m}^{\mathrm{NLoS}}(t)=\bar{\theta}_{\mathrm{tx/rx}}(t)+\Delta\theta_{\mathrm{tx/rx}}, \quad (26)$$

$$\phi_{\mathrm{tx/rx},n,m}^{\mathrm{NLoS}}(t)=\bar{\phi}_{\mathrm{tx/rx}}(t)+\Delta\phi_{\mathrm{tx/rx}}, \quad (27)$$

where $\Delta\theta$ and $\Delta\phi$ are the angle offsets of elevation and azimuth, respectively.

Substituting (26) and (27) into (23), the theoretical ACF can be obtained as (28), as shown at the bottom of the page. Under the condition of 2D scattering scenario, the ACF can also be rewritten as (29), as shown at the bottom of the page. Furthermore, during the short time period, the speed, the movement direction, and the mean angle can be viewed as changing linearly, and the theoretical ACF of proposed model with velocity variation can be further expressed as

$$r_{\varsigma\dot{\varsigma}}(t,\Delta t)=\frac{1}{2\pi I_0(\kappa)}\cdot\int_{-\pi}^{+\pi}\mathrm{e}^{jkM(t,\Delta t)\sin\Delta\phi_{tx}+(\kappa+jkN(t,\Delta t)\cos\Delta\phi_{tx})}d\Delta\phi_{tx} \quad (30)$$

$$f_{n,m}^{\mathrm{NLoS}}(t)=\frac{1}{\lambda}\left(\|\mathbf{v}_{\mathrm{tx}}(t)\|\begin{bmatrix}\cos\alpha_{\mathrm{tx}}(t)\\ \sin\alpha_{\mathrm{tx}}(t)\\ 0\end{bmatrix}^{T}\cdot\begin{bmatrix}\cos\theta_{\mathrm{tx},n,m}^{\mathrm{NLoS}}(t)\cos\phi_{\mathrm{tx},n,m}^{\mathrm{NLoS}}(t)\\ \cos\theta_{\mathrm{tx},n,m}^{\mathrm{NLoS}}(t)\sin\phi_{\mathrm{tx},n,m}^{\mathrm{NLoS}}(t)\\ \sin\theta_{\mathrm{tx},n,m}^{\mathrm{NLoS}}(t)\end{bmatrix}\right.$$
$$\left.+\ \|\mathbf{v}_{\mathrm{rx}}(t)\|\begin{bmatrix}\cos\alpha_{\mathrm{rx}}(t)\\ \sin\alpha_{\mathrm{rx}}(t)\\ 0\end{bmatrix}^{T}\cdot\begin{bmatrix}\cos\theta_{\mathrm{rx},n,m}^{\mathrm{NLoS}}(t)\cos\phi_{\mathrm{rx},n,m}^{\mathrm{NLoS}}(t)\\ \cos\theta_{\mathrm{rx},n,m}^{\mathrm{NLoS}}(t)\sin\phi_{\mathrm{rx},n,m}^{\mathrm{NLoS}}(t)\\ \sin\theta_{\mathrm{rx},n,m}^{\mathrm{NLoS}}(t)\end{bmatrix}\right) \quad (20)$$

$$r_{\varsigma\dot{\varsigma}}(t,\Delta t)=\iint\iint\sqrt{p\left(\theta_{n,m}^{\mathrm{NLoS}}(t+\Delta t),\phi_{n,m}^{\mathrm{NLoS}}(t+\Delta t)\right)}\sqrt{p\left(\theta_{n,m}^{\mathrm{NLoS}}(t),\phi_{n,m}^{\mathrm{NLoS}}(t)\right)}$$
$$\cdot\mathrm{e}^{jk\int_{t}^{t+\Delta t}(\mathbf{v}_{\mathrm{tx}}(\tau)\cdot\mathbf{s}_{\mathrm{tx},n,m}(\tau)+\mathbf{v}_{\mathrm{rx}}(\tau)\cdot\mathbf{s}_{\mathrm{rx},n,m}(\tau))d\tau}d\theta_{n,m}^{\mathrm{NLoS}}(t+\Delta t)\,d\theta_{n,m}^{\mathrm{NLoS}}(t)\,d\phi_{n,m}^{\mathrm{NLoS}}(t+\Delta t)\,d\phi_{n,m}^{\mathrm{NLoS}}(t) \quad (23)$$

$$r_{\varsigma\dot{\varsigma}}(t,\Delta t)=\iint\iint\sqrt{\frac{e^{\kappa\cos\Delta\phi_{\mathrm{tx}}-|\Delta\theta_{\mathrm{tx}}|/\sigma}}{4\pi\sigma I_0(\kappa)}}\sqrt{\frac{e^{\kappa\cos\Delta\phi_{\mathrm{rx}}-|\Delta\theta_{\mathrm{rx}}|/\sigma}}{4\pi\sigma I_0(\kappa)}}$$
$$\cdot\mathrm{e}^{jk\int_{t}^{t+\Delta t}\|\mathbf{v}_{\mathrm{tx}}(t)\|\left(\cos\beta_{\mathrm{tx}}(\tau)\cos\left(\bar{\theta}_{\mathrm{tx}}(\tau)+\Delta\theta_{\mathrm{tx}}\right)\cos\left[\alpha_{\mathrm{tx}}(\tau)-\bar{\phi}_{\mathrm{tx}}(\tau)-\Delta\phi_{\mathrm{tx}}\right]+\sin\beta_{\mathrm{tx}}(\tau)\sin\left(\bar{\theta}_{\mathrm{tx}}(\tau)+\Delta\theta_{\mathrm{tx}}\right)\right)d\tau}$$
$$\cdot\mathrm{e}^{jk\int_{t}^{t+\Delta t}\|\mathbf{v}_{\mathrm{rx}}(t)\|\left(\cos\beta_{\mathrm{rx}}(\tau)\cos\left(\bar{\theta}_{\mathrm{rx}}(\tau)+\Delta\theta_{\mathrm{rx}}\right)\cos\left[\alpha_{\mathrm{rx}}(\tau)-\bar{\phi}_{\mathrm{rx}}(\tau)-\Delta\phi_{\mathrm{rx}}\right]+\sin\beta_{\mathrm{rx}}(\tau)\sin\left(\bar{\theta}_{\mathrm{rx}}(\tau)+\Delta\theta_{\mathrm{rx}}\right)\right)d\tau}$$
$$d\bar{\theta}_{\mathrm{tx}}(t+\Delta t)\,d\bar{\theta}_{\mathrm{rx}}(t)\,d\bar{\phi}_{\mathrm{tx}}(t+\Delta t)\,d\phi_{\mathrm{rx}}(t) \quad (28)$$

$$r_{\varsigma\dot{\varsigma}}(t,\Delta t)=\int_{-\pi}^{+\pi}\frac{\mathrm{e}^{\kappa\cos\Delta\phi_{tx}}}{2\pi I_0(\kappa)}\mathrm{e}^{jk\int_{t}^{t+\Delta t}\|\mathbf{v}_{\mathrm{tx}}(\tau)\|\cos(\alpha_{tx}(\tau)-\bar{\phi}_{tx}(\tau)-\Delta\phi_{tx})d\tau}d\Delta\phi_{tx} \quad (29)$$

where $M(t, \Delta t)$ and $N(t, \Delta t)$ are given in (31) and (32), as shown at the bottom of the page, respectively, a_{tx}, $\omega_{\phi}^{\mathrm{tx}}$, and C_{ϕ}^{tx} represent the changing rates of velocity, direction, and AAoD, respectively, $v_{\mathrm{tx}}(t_0)$, $\alpha_{\mathrm{tx}}(t_0)$, and $\phi_{\mathrm{tx}}(t_0)$ denote the initial values of velocity, direction, and AAoD, respectively. Finally, according to the integral formula of [35, Eq.(3.338-4)], the ACF can be further simplified as

$$r_{\varsigma\dot{\varsigma}}(t, \Delta t) = \frac{I_0\left(\sqrt{(jkM(t, \Delta t))^2 + (\kappa + jkN(t, \Delta t))}\right)}{2\pi I_0(\kappa)} = \frac{I_0\left(\sqrt{Q(t, \Delta t)}\right)}{2\pi I_0(\kappa)}, \tag{33}$$

where $Q(t, \Delta t)$ is given as (34), as shown at the bottom of the page.

D. THEORETICAL LCR AND AFD

The LCR denotes the expected rate at which the signal envelope passes through the specified level with a positive or negative slope within one second, and the AFD means the average duration where the amplitude of fading envelope remains below a given threshold. According to the definitions, LCR and AFD can be calculated respectively by

$$N(t, r) = \int_0^{+\infty} \dot{r} p_{\varsigma\dot{\varsigma}}(t, r, \dot{r}) d\dot{r}, \tag{35}$$

$$T(t, r) = \frac{P_{\xi}(t, r)}{N(t, r)}, \tag{36}$$

where r means the level of threshold. Substituting (15) into (35), the theoretical LCR of proposed model can be obtained as (37), as shown at the bottom of the next page.

$$\begin{aligned} M(t, \Delta t) = {} & \frac{2(v_{\mathrm{tx}}(t_0) + a_{\mathrm{tx}}t)\sin\left[\left(\omega_{\phi}^{\mathrm{tx}} - C_{\phi}^{\mathrm{tx}}\right)(t + \Delta t/2) + \alpha_{\mathrm{tx}}(t_0) - \phi_{\mathrm{tx}}(t_0)\right]\sin\left[\left(\omega_{\phi}^{\mathrm{tx}} - C_{\phi}^{\mathrm{tx}}\right)\Delta t/2\right]}{\omega_{\phi}^{\mathrm{tx}} - C_{\phi}^{\mathrm{tx}}} \\ & + \frac{2a_{\mathrm{tx}}t\cos\left[\left(\omega_{\phi}^{\mathrm{tx}} - C_{\phi}^{\mathrm{tx}}\right)(t + \Delta t/2) + \alpha_{\mathrm{tx}}(t_0) - \phi_{\mathrm{tx}}(t_0)\right]\sin\left[\left(\omega_{\phi}^{\mathrm{tx}} - C_{\phi}^{\mathrm{tx}}\right)\Delta t/2\right]}{\left(\omega_{\phi}^{\mathrm{tx}} - C_{\phi}^{\mathrm{tx}}\right)^2} \\ & - \frac{a_{\mathrm{tx}}\Delta t\cos\left[\left(\omega_{\phi}^{\mathrm{tx}} - C_{\phi}^{\mathrm{tx}}\right)(t + \Delta t) + \alpha_{\mathrm{tx}}(t_0) - \phi_{\mathrm{tx}}(t_0)\right]}{\omega_{\phi}^{\mathrm{tx}} - C_{\phi}^{\mathrm{tx}}} \end{aligned} \tag{31}$$

$$\begin{aligned} N(t, \Delta t) = {} & \frac{2(v_{\mathrm{tx}}(t_0) + a_{\mathrm{tx}}t)\cos\left[\left(\omega_{\phi}^{\mathrm{tx}} - C_{\phi}^{\mathrm{tx}}\right)(t + \Delta t/2) + \alpha_{\mathrm{tx}}(t_0) - \phi_{\mathrm{tx}}(t_0)\right]\sin\left[\left(\omega_{\phi}^{\mathrm{tx}} - C_{\phi}^{\mathrm{tx}}\right)\Delta t/2\right]}{\omega_{\phi}^{\mathrm{tx}} - C_{\phi}^{\mathrm{tx}}} \\ & + \frac{2a_{\mathrm{tx}}t\sin\left[\left(\omega_{\phi}^{\mathrm{tx}} - C_{\phi}^{\mathrm{tx}}\right)(t + \Delta t/2) + \alpha_{\mathrm{tx}}(t_0) - \phi_{\mathrm{tx}}(t_0)\right]\sin\left[\left(\omega_{\phi}^{\mathrm{tx}} - C_{\phi}^{\mathrm{tx}}\right)\Delta t/2\right]}{\left(\omega_{\phi}^{\mathrm{tx}} - C_{\phi}^{\mathrm{tx}}\right)^2} \\ & - \frac{a_{\mathrm{tx}}\Delta t\sin\left[\left(\omega_{\phi}^{\mathrm{tx}} - C_{\phi}^{\mathrm{tx}}\right)(t + \Delta t) + \alpha_{\mathrm{tx}}(t_0) - \phi_{\mathrm{tx}}(t_0)\right]}{\omega_{\phi}^{\mathrm{tx}} - C_{\phi}^{\mathrm{tx}}} \end{aligned} \tag{32}$$

$$\begin{aligned} Q(t, \Delta t) = {} & \kappa^2 + j2kN(t, \Delta t) - k^2M^2(t, \Delta t) - k^2N^2(t, \Delta t) \\ = {} & \kappa^2 + j2k\left(\begin{array}{l} \frac{2(v_{\mathrm{tx}}(t_0) + a_{\mathrm{tx}}t)\cos\left[\left(\omega_{\phi}^{\mathrm{tx}} - C_{\phi}^{\mathrm{tx}}\right)(t + \Delta t/2) + \alpha_{\mathrm{tx}}(t_0) - \phi_{\mathrm{tx}}(t_0)\right]\sin\left[\left(\omega_{\phi}^{\mathrm{tx}} - C_{\phi}^{\mathrm{tx}}\right)\Delta t/2\right]}{\omega_{\phi}^{\mathrm{tx}} - C_{\phi}^{\mathrm{tx}}} \\ + \frac{2a_{\mathrm{tx}}t\sin\left[\left(\omega_{\phi}^{\mathrm{tx}} - C_{\phi}^{\mathrm{tx}}\right)(t + \Delta t/2) + \alpha_{\mathrm{tx}}(t_0) - \phi_{\mathrm{tx}}(t_0)\right]\sin\left[\left(\omega_{\phi}^{\mathrm{tx}} - C_{\phi}^{\mathrm{tx}}\right)\Delta t/2\right]}{\left(\omega_{\phi}^{\mathrm{tx}} - C_{\phi}^{\mathrm{tx}}\right)^2} \\ - \frac{a_{\mathrm{tx}}\Delta t\sin\left[\left(\omega_{\phi}^{\mathrm{tx}} - C_{\phi}^{\mathrm{tx}}\right)(t + \Delta t) + \alpha_{\mathrm{tx}}(t_0) - \phi_{\mathrm{tx}}(t_0)\right]}{\omega_{\phi}^{\mathrm{tx}} - C_{\phi}^{\mathrm{tx}}} \end{array}\right) \\ & - k^2\left(\begin{array}{l} \frac{4(v_{\mathrm{tx}}(t_0) + a_{\mathrm{tx}}t)^2\sin^2\left[\left(\omega_{\phi}^{\mathrm{tx}} - C_{\phi}^{\mathrm{tx}}\right)\Delta t/2\right] + a_{\mathrm{tx}}{}^2\Delta t^2 + 2(v_{\mathrm{tx}}(t_0) + a_{\mathrm{tx}}t)\sin^2\left[\left(\omega_{\phi}^{\mathrm{tx}} - C_{\phi}^{\mathrm{tx}}\right)\Delta t/2\right]}{\left(\omega_{\phi}^{\mathrm{tx}} - C_{\phi}^{\mathrm{tx}}\right)^2} \\ + \frac{4a_{\mathrm{tx}}{}^2t^2\sin^2\left[\left(\omega_{\phi}^{\mathrm{tx}} - C_{\phi}^{\mathrm{tx}}\right)\Delta t/2\right]}{\left(\omega_{\phi}^{\mathrm{tx}} - C_{\phi}^{\mathrm{tx}}\right)^4} - \frac{2a_{\mathrm{tx}}{}^2\Delta t\sin\left[\left(\omega_{\phi}^{\mathrm{tx}} - C_{\phi}^{\mathrm{tx}}\right)\Delta t/2\right]\cos\left[\left(\omega_{\phi}^{\mathrm{tx}} - C_{\phi}^{\mathrm{tx}}\right)\Delta t/2\right]}{\left(\omega_{\phi}^{\mathrm{tx}} - C_{\phi}^{\mathrm{tx}}\right)^3} \end{array}\right) \end{aligned} \tag{34}$$

It can be proved that when the path number M approaches infinity, the expression would be

$$N(t,r)=\sqrt{\frac{R(t)}{2\pi}}p_{\varsigma}(r), \tag{38}$$

where $R(t)$ is the second derivative of ACF with $\Delta t=0$, and defined by

$$R(t)=\frac{\partial^2 r_{\varsigma\dot{\varsigma}}(t,\Delta t)}{\partial \Delta t^2}|_{\Delta t=0}. \tag{39}$$

Similarly, $P_{\varsigma}(t,r)$ is the CDF of ς and can be obtained by substituting (14) into $P_{\varsigma}(t,r)=\int_0^r p_{\varsigma}(r)dr$. When M approaches infinity, we can get the theoretical expression of AFD as

$$T(t,r)=\frac{1-Q\left(\sqrt{2K_R(t)},\sqrt{2\left(K_R(t)+1\right)r^2}\right)}{N(t,r)}. \tag{40}$$

IV. SIMULATION RESULTS AND ANALYZE

In this section, based on the derived expressions of LCR and AFD of proposed model, the numerical simulations are investigated and compared with the theoretical and measured data. Since the statistical properties of stochastic model vary with each single simulation, the simulation results in this section are based on the average value of 1500 simulations. The carrier frequency is 2.4 GHz and the initial distance between the UAV and vehicle is 150 m. The UAV flies away from the vehicle. The Ricean factor obeys a Gaussian distribution $K_R(t)\sim N(1,3)$. For general purpose, the environment dependant parameters are set as $H=50$ m, $R=10$ m. Both the elevation and azimuth are supposed to obey the Laplacian distribution with $\sigma=\pi/6$ and VM distributions with $\kappa=10$ [37]. The 3D velocities of UAV and vehicle are modeled as

$$\|\mathbf{v}_{\mathrm{tx/rx}}(t)\|=v_{\mathrm{tx/rx}}(t_0)+a_{\mathrm{tx/rx}}t, \tag{41a}$$
$$\bar{\theta}_{\mathrm{tx/rx}}(t)=\omega_{\theta}^{\mathrm{tx/rx}}t+C_{\theta}^{\mathrm{tx/rx}}, \tag{41b}$$
$$\bar{\phi}_{\mathrm{tx/rx}}(t)=\omega_{\phi}^{\mathrm{tx/rx}}t+C_{\phi}^{\mathrm{tx/rx}}. \tag{41c}$$

The parameters are given in Table 2. Fig. 2 shows the corresponding trajectories based on these parameters and the initial locations of cluster within one simulation.

In order to demonstrate the time fluctuation of fading envelope for the undergoing UAV channel, the theoretical expressions based on the above derivation and simulation results of LCR and AFD under the 3D flight scenario at t = 0.5s, 1s and 1.5s are shown in Fig. 3 and Fig. 4, respectively. It clearly shows that the theoretical values are consistent with the simulated ones, which verifies the derivations as well as the simulations. In addition, both of two figures show

TABLE 2. Parameters of 3D velocity.

Parameter	Value	Parameter	Value
$v_{\mathrm{tx}}(t_0)\,(m/s)$	20	$v_{\mathrm{rx}}(t_0)\,(m/s)$	3
$a_{\mathrm{tx}}\,(m/s^2)$	3	$a_{\mathrm{rx}}\,(m/s^2)$	1
$\omega_{\theta}^{\mathrm{tx}}\,(^\circ/s)$	1	$\omega_{\theta}^{\mathrm{rx}}\,(^\circ/s)$	0.2
$\omega_{\phi}^{\mathrm{tx}}\,(^\circ/s)$	2	$\omega_{\phi}^{\mathrm{rx}}\,(^\circ/s)$	0.5
$C_{\theta}^{\mathrm{tx}}\,(^\circ)$	30	$C_{\theta}^{\mathrm{rx}}\,(^\circ)$	20
$C_{\phi}^{\mathrm{tx}}\,(^\circ)$	20	$C_{\phi}^{\mathrm{rx}}\,(^\circ)$	15

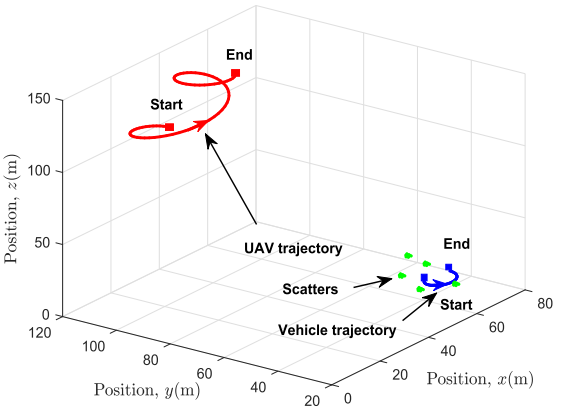

FIGURE 2. 3D Trajectories of the UAV and vehicle.

that the LCR and AFD change over time, which includes the important non-stationary aspect due to the movements of transceivers and scatterers.

To the best knowledge of authors, there are few measurement results of LCR and AFD for UAV channels. In [36], the authors carried out some measurements on the statistical properties of UAV channels in the urban environment. In order to verify the correctness of proposed model, we adjust the simulation parameters according to the field test condition in [36], where the speed of UAV is 8 m/s, the initial distance between the UAV and vehicle is 1000 m. The comparisons between the theoretical LCR and AFD with the measured data are shown in Fig. 5. The consistency in the figure verifies the validity of proposed model.

To investigate the effect of cluster's position on the LCR and AFD, we assume that the local clusters distribute on the surface of serval cylinders with different heights and radiuses. The center of cylinder is set as the starting point of the vehicle

$$N(t,r)=4\pi r\int_0^{\dot{z}_{\max}}\dot{r}\int_0^{\infty}\int_0^{\infty}\int_0^{2\pi}\left[\prod_{m=1}^{M}J_0\left(2\pi\frac{1}{\sqrt{m}}\left\{r_1{}^2+(2\pi\dot{\Phi}^{\mathrm{NLoS}}(t)r_2)^2\right.\right.\right.$$
$$\left.\left.\left.-4\pi\dot{\Phi}^{\mathrm{NLoS}}(t)r_1r_2\sin\theta\right\}^{\frac{1}{2}}\right)\right]\cdot \mathrm{e}^{-j2\pi[rr_1\cos\theta+\dot{z}r_2]}r_1d\theta dr_1dr_2d\dot{r} \tag{37}$$

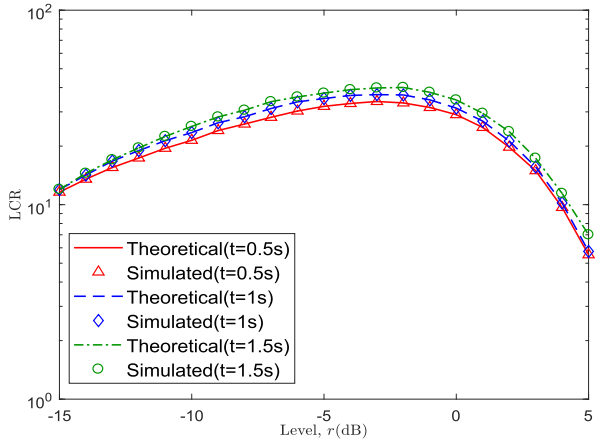

FIGURE 3. Theoretical and simulated LCRs at different time instants.

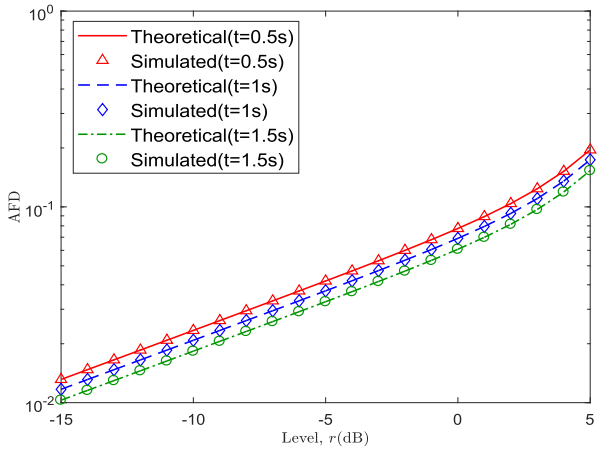

FIGURE 4. Theoretical and simulated AFDs at different time instants.

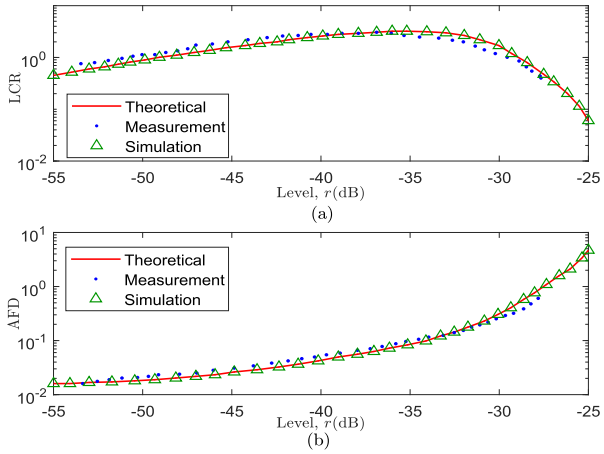

FIGURE 5. Theoretical, measured, and simulated (a) LCRs and (b) AFDs.

in the simulation. The typical heights are 2 m, 10 m, and 50 m and the typical radiuses are 5 m, 10 m, and 20 m. The LCRs and AFDs with different heights and radiuses are shown in Fig. 6 and Fig. 7, respectively. As we can see that the

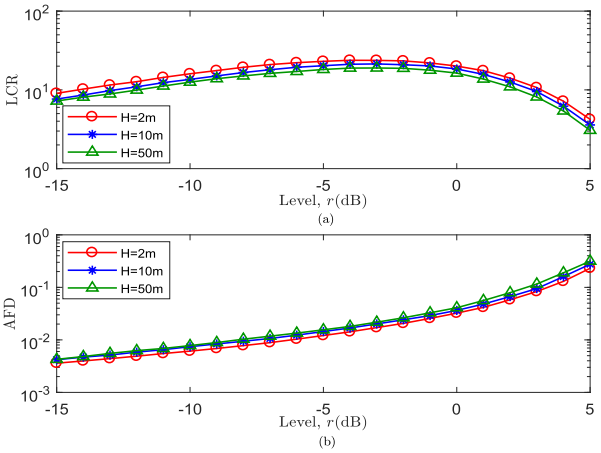

FIGURE 6. Effects of cluster's height on the (a) LCRs and (b) AFDs.

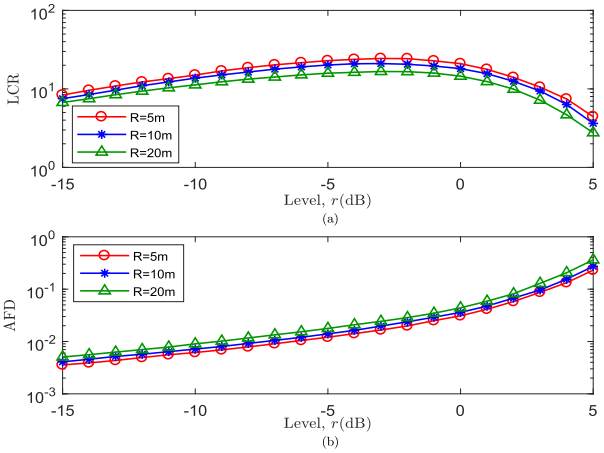

FIGURE 7. Effects of cluster's radius on the (a) LCRs and (b) AFDs.

LCR decreases while the AFD increases as the distance value increases, which means the fluctuation of received signal is more severe. Meanwhile, under the UAV communication scenarios, the scattering scenario changes as the transmitter and receiver moving. When the threshold level increases, the fading envelope tends to be smaller than the level in most of time. The rate of fading envelope breaks through the level decreases, while the average duration of fading envelope below the level increases. Thus, the LCR decreases while the AFD increases as the threshold level increases.

V. CONCLUSION

In this paper, we have developed a generic 3D non-stationary cylinder-based GBSM for UAV channels. Considering the specific scenario of UAV-to-ground communications, the proposed model includes the LoS and NLoS components and takes the 3D movements and 3D scattering into account. Based on the proposed model, the theoretical expressions of two important statistical properties, i.e., LCR and AFD, have been analyzed and derived in details. These expressions have also been validated by the simulations and the measured

results under the urban environment. It should be mentioned that channel fading has a significant impact on the quality and reliability of signal transmission and the analytical LCR and AFD can well describe the fading rate. Thus, the derived expressions are of great significance to channel coding, block interleave, and system design. In the future, we will carry out measurements of UAV channels under different environments to further optimize the angle distributions and verify the theoretical results.

REFERENCES

[1] Y. Zeng, R. Zhang, and T. J. Lim, "Wireless communications with unmanned aerial vehicles: Opportunities and challenges," *IEEE Commun. Mag.*, vol. 54, no. 5, pp. 36–42, May 2016.

[2] C.-X. Wang, J. Bian, J. Sun, W. Zhang, and M. Zhang, "A survey of 5G channel measurements and models," *IEEE Commun. Surveys Tuts.*, vol. 20, no. 4, pp. 3142–3168, Aug. 2018.

[3] J. Zhang, M. Shafi, A. F. Molisch, F. Tufvesson, S. Wu, and K. Kitao, "Channel models and measurements for 5G," *IEEE Commun. Mag.*, vol. 56, no. 12, pp. 12–13, Dec. 2018.

[4] D. W. Matolak, "Air-ground channels & models: Comprehensive review and considerations for unmanned aircraft systems," in *Proc. IEEE Aerosp. Conf.*, Big Sky, MT, USA, Mar. 2012, pp. 1–17.

[5] J. Zheng, J. Zhang, S. Chen, H. Zhao, and B. Ai, "Wireless powered UAV relay communications over fluctuating two-ray fading channels," *Phys. Commun.*, vol. 35, Aug. 2019, Art. no. 100724.

[6] Q. Zhu, S. Jiang, C.-X. Wang, B. Hua, K. Mao, X. Chen, and W. Zhong, "Effects of digital map on the RT-based channel model for UAV mmWave communications," in *Proc. Int. Wireless Commun. Mobile Comput. (IWCMC)*, Limassol, Cyprus, Jun. 2020, pp. 1–6.

[7] M. Mozaffari, W. Saad, M. Bennis, and M. Debbah, "Wireless communication using unmanned aerial vehicles (UAVs): Optimal transport theory for hover time optimization," *IEEE Trans. Wireless Commun.*, vol. 16, no. 12, pp. 8052–8066, Dec. 2017.

[8] M. Mozaffari, W. Saad, M. Bennis, and M. Debbah, "Mobile unmanned aerial vehicles (UAVs) for energy-efficient Internet of Things communications," *IEEE Trans. Wireless Commun.*, vol. 16, no. 11, pp. 7574–7589, Nov. 2017.

[9] K. Jiang, X. Chen, Q. Zhu, W. Zhong, Y. Wang, X. Yu, and B. Chen, "A geometry-based 3D non-stationary UAV-MIMO channel model allowing 3D arbitrary trajectories," in *Proc. 10th Int. Conf. Wireless Commun. Signal Process. (WCSP)*, Hangzhou, China, Oct. 2018, pp. 1–6.

[10] Q. Zhu, Y. Wang, K. Jiang, X. Chen, W. Zhong, and N. Ahmed, "3D non-stationary geometry-based multi-input multi-output channel model for UAV-ground communication systems," *IET Microwav., Antennas Propag.*, vol. 13, no. 8, pp. 1104–1121, June. 2019.

[11] H. Chang, J. Bian, C.-X. Wang, Z. Bai, J. Sun, and X. Gao, "A 3D wideband geometry-based stochastic model for UAV Air-to-Ground channels," in *Proc. IEEE Global Commun. Conf. (GLOBECOM)*, Abu Dhabi, United Arab Emirates, Dec. 2018, pp. 206–212.

[12] W. Fan, X. Carreno Bautista de Lisbona, F. Sun, J. O. Nielsen, M. B. Knudsen, and G. F. Pedersen, "Emulating spatial characteristics of MIMO channels for OTA testing," *IEEE Trans. Antennas Propag.*, vol. 61, no. 8, pp. 4306–4314, Aug. 2013.

[13] Z. Cui, C. Briso, K. Guan, D. W. Matolak, C. Calvo-Ramírez, B. Ai, and Z. Zhong, "Low-altitude UAV air-ground propagation channel measurement and analysis in a suburban environment at 3.9 GHz," *IET Microwav., Antennas Propag.*, vol. 13, no. 9, pp. 1503–1508, Jul. 2019.

[14] Y. Wu, Z. Gao, C. Chen, L. Huang, H.-P. Chiang, Y.-M. Huang, and H. Sun, "Ray tracing based wireless channel modeling over the sea surface near Diaoyu Islands," in *Proc. 1st Int. Conf. Comput. Intell. Theory, Syst. Appl. (CCITSA)*, Yilan, Taiwan, Dec. 2015, pp. 124–128.

[15] E. Greenberg and P. Levy, "Channel characteristics of UAV to ground links over multipath urban environments," in *Proc. IEEE Int. Conf. Microw., Antennas, Commun. Electron. Syst. (COMCAS)*, Tel-Aviv, Israel, Nov. 2017, pp. 1–4.

[16] W. Khawaja, O. Ozdemir, and I. Guvenc, "UAV Air-to-Ground channel characterization for mmWave systems," in *Proc. IEEE 86th Veh. Technol. Conf. (VTC-Fall)*, Toronto, ON, Canada, Sep. 2017, pp. 1–5.

[17] Z. Shi, P. Xia, C. Chen, L. Huang, and Z. Gao, "Modeling of wireless channel between UAV and vessel using the FDTD method," in *Proc. 10th Int. Conf. Wireless Commun., Netw. Mobile Comput. (WiCOM)*, Beijing, China, Sep. 2014, pp. 362–377.

[18] N. Goddemeier and C. Wietfeld, "Investigation of air-to-air channel characteristics and a UAV specific extension to the rice model," in *Proc. IEEE Globecom Workshops (GC Wkshps)*, San Diego, CA, USA, Dec. 2015, pp. 1–5.

[19] M. Yang, S. Zhang, X. Shao, Q. Guo, and W. Tang, "Statistical modeling of the high altitude platform dual-polarized MIMO propagation channel," *China Commun.*, vol. 14, no. 3, pp. 43–54, Mar. 2017.

[20] J. Li, X. Zhang, R. Cao, and M. Zhou, "Reduced-dimension MUSIC for angle and array gain-phase error estimation in bistatic MIMO radar," *IEEE Commun. Lett.*, vol. 17, no. 3, pp. 443–446, Mar. 2013.

[21] B. Yao, X. Li, L. Shi, Y. Liu, and C. Zhu, "A geometric-stochastic integrated channel model for hypersonic vehicle: A physical perspective," *IEEE Trans. Veh. Technol.*, vol. 68, no. 5, pp. 4328–4344, May 2019.

[22] D. W. Matolak and R. Sun, "Air–ground channel characterization for unmanned aircraft systems—Part I: Methods, measurements, and models for over-water settings," *IEEE Trans. Veh. Technol.*, vol. 66, no. 1, pp. 26–44, Jan. 2017.

[23] L. Zeng, X. Cheng, C.-X. Wang, and X. Yin, "A 3D geometry-based stochastic channel model for UAV-MIMO channels," in *Proc. IEEE Wireless Commun. Netw. Conf. (WCNC)*, San Francisco, CA, USA, Mar. 2017, pp. 1–5.

[24] Z. Lian, L. Jiang, and C. He, "A 3-D wideband model based on dynamic evolution of scatterers for HAP-MIMO channel," *IEEE Commun. Lett.*, vol. 21, no. 3, pp. 684–687, Mar. 2017.

[25] J. Hu, L. Jiang, C. He, Z. Lian, and J. Liu, "A 3-D HAP-MIMO channel model based on dynamic properties of scatterers," in *Proc. 9th Int. Conf. Wireless Commun. Signal Process. (WCSP)*, Nanjing, China, Oct. 2017, pp. 1–5.

[26] S. Gulfam, S. Nawaz, A. Ahmed, M. Patwary, and Q. Ni, "A novel 3D analytical scattering model for air-to-ground fading channels," *Appl. Sci.*, vol. 6, no. 8, p. 207, Aug. 2016.

[27] L. Zeng, X. Cheng, C.-X. Wang, and X. Yin, "Second order statistics of non-isotropic UAV Ricean fading channels," in *Proc. IEEE 86th Veh. Technol. Conf. (VTC-Fall)*, Toronto, ON, Canada, Sep. 2017, pp. 1–5.

[28] R. Jia, Y. Li, X. Cheng, and B. Ai, "3D geometry-based UAV-MIMO channel modeling and simulation," *China Commun.*, vol. 15, no. 12, pp. 67–74, Dec. 2018.

[29] Y. Wang, N. Cheng, X. Chen, W. Fan, Q. Zhu, and W. Zhong, "On the second order statistics of 3D non-stationary UAV channels allowing velocity variations," in *Proc. 14th Eur. Conf. Antennas Propag. (EuCAP)*, Copenhagen, Denmark, Mar. 2020, pp. 1–5.

[30] Q. Zhu, Y. Wang, K. Jiang, X. Chen, W. Zhong, and N. Ahmed, "3D non-stationary geometry-based MIMO channel model for UAV-ground communication systems," *IET Microwav. Antennas Propag.*, vol. 13, no. 8, pp. 1104–1112, Jun. 2019.

[31] M. Pätzold and B. Talha, "On the statistical properties of sum-of-cisoids-based mobile radio channel models," in *Proc. 10th Int. Symp. Wireless Pers. Multimedia Commun. (WPMC)*, Jaipur, India, Dec. 2007, pp. 394–400.

[32] A. Ghazal, Y. Yuan, C.-X. Wang, Y. Zhang, Q. Yao, H. Zhou, and W. Duan, "A non-stationary IMT-advanced MIMO channel model for high-mobility wireless communication systems," *IEEE Trans. Wireless Commun.*, vol. 16, no. 4, pp. 2057–2068, Apr. 2017.

[33] Q. Zhu, Y. Yang, X. Chen, Y. Tan, Y. Fu, C.-X. Wang, and W. Li, "A novel 3D non-stationary vehicle-to-vehicle channel model and its spatial-temporal correlation properties," *IEEE Access*, vol. 6, pp. 43633–43643, Jul. 2018.

[34] W. Khawaja, I. Guvenc, D. W. Matolak, U.-C. Fiebig, and N. Schneckenburger, "A survey of air-to-ground propagation channel modeling for unmanned aerial vehicles," *IEEE Commun. Surveys Tuts.*, vol. 21, no. 3, pp. 2361–2391, 3rd Quart., 2019.

[35] I. S. Gradshteyn and I. M. Ryzhik, *Table of Integrals, Series, and Products*. New York, NY, USA: Academic, 2014.

[36] M. Simunek, F. P. Fontan, and P. Pechac, "The UAV low elevation propagation channel in urban areas: Statistical analysis and time-series generator," *IEEE Trans. Antennas Propag.*, vol. 61, no. 7, pp. 3850–3858, Jul. 2013.

[37] Z. Lian, L. Jiang, C. He, and Q. Xi, "A novel channel model for 3-D HAP-MIMO communication systems," in *Proc. Int. Conf. Netw. Netw. Appl. (NaNA)*, Hakodate, Japan, Jul. 2016, pp. 1–6.

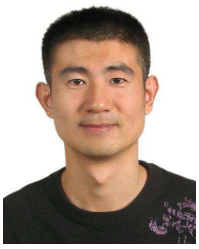

QIUMING ZHU (Member, IEEE) received the B.S. degree in electronic engineering from the Nanjing University of Aeronautics and Astronautics (NUAA), Nanjing, China, in 2002, and the M.S. and Ph.D. degrees in communication and information systems, in 2005 and 2012, respectively. Since 2012, he has been an Associate Professor of wireless communications with NUAA. From 2016 to 2017, he was a Visiting Academic with Heriot-Watt University. His research interests include channel modeling for 5G communication systems and wireless channel emulators.

NENG CHENG received the B.S. degree in electronic information science and technology from Jilin University, Changchun, China, in 2018. He is currently pursuing the M.S. degree in signal and information processing with the Nanjing University of Aeronautics and Astronautics. His research interests include unmanned aerial vehicle channel modeling and channel measurement.

XIAOMIN CHEN (Member, IEEE) received the B.S. degree in electronic engineering and the M.S. and Ph.D. degrees in communication and information systems from the Nanjing University of Aeronautics and Astronautics (NUAA), Nanjing, China, in 1997, 2001, and 2010, respectively. Since 2010, she has been an Associate Professor with NUAA. Her research interests include adaptive techniques for next-generation mobile communication systems and MIMO channel models.

WEIZHI ZHONG (Member, IEEE) received the B.S. and M.S. degrees in communication and information system from Jilin University, Changchun, China, in 2003 and 2006, respectively, and the Ph.D. degree in communication and information system from the Harbin Institute of Technology, Harbin, China, in 2010. Since 2010, she has been an Associate Professor with the College of Astronautics, NUAA. Her research interests include millimeter-wave communication and MIMO technique. She is a member of the Chinese Institute of Aeronautics.

BOYU HUA received the B.S. degree in physics from Nanjing Normal University, China, in 2014, and the M.S. degree in electronic communication engineering from the Nanjing University of Aeronautics and Astronautics (NUAA), China, in 2018, where he is currently pursuing the Ph.D. degree in communication and information systems. Since 2018, he has been an Experimentalist with NUAA. His research interests include wireless channel modeling for 5G and B5G communication.

YAWEN WANG received the B.S. degree in electronic information science and technology from Jilin University, Changchun, China, in 2017. He is currently pursuing the M.S. degree in signal and information processing with the Nanjing University of Aeronautics and Astronautics. His research interests include unmanned aerial vehicle channel modeling and channel measurement.